Chinese Chemical Letters 35 (2024) 108470

Contents lists available at ScienceDirect

Chinese Chemical Letters

journal homepage: www.elsevier.com/locate/cclet

Designing ABC-6 family small pore zeolites by epitaxial growth approach

Xiaohui Cui[a,b,1], Jia Lv[c,1], Chao Ma[b,d], Yujiao Wang[c], Zhenghao Jia[e], Daliang Zhang[c,*], Peng Guo[b,d,*], Zhongmin Liu[a,b,d]

[a] Henan Institute of Advanced Technology, Zhengzhou University, Zhengzhou 450001, China
[b] National Engineering Research Center of Lower-Carbon Catalysis Technology, Dalian Institute of Chemical Physics, Chinese Academy of Sciences, Dalian 116023, China
[c] Multi-scale Porous Materials Center, Institute of Advanced Interdisciplinary Studies & School of Chemistry Engineering, Chongqing University, Chongqing 400044, China
[d] University of Chinese Academy of Sciences, Beijing 100049, China
[e] Division of Energy Research Resources, Dalian Institute of Chemical Physics, Chinese Academy of Sciences, Dalian 116023, China

ARTICLE INFO

Article history:
Received 4 March 2023
Revised 3 April 2023
Accepted 18 April 2023
Available online 21 April 2023

Keywords:
Zeolite structure
Zeolite synthesis
Structural characterizations
Low-dose imaging
Focused ion beam

ABSTRACT

Aluminosilicate small pore zeolites belonging to ABC-6 family play crucially important roles in the high methanol conversion with the high selectivity of light olefins, gas separation and storage, and selective catalytic reduction of NO_x. In this work, we report a general method, called the epitaxial growth approach, for designing ABC-6 family small pore zeolites. It is mainly realized through the epitaxial growth on the nonporous **SOD**-type zeolite in the presence of inorganic cations (Na^+ and K^+) combined with a variety of organic structure directing agents (OSDAs). In this case, a series of ABC-6 family small pore zeolites such as **ERI-**, **SWY-**, **LEV-**, **AFX-**, and **PTT-**type zeolites have been successfully synthesized within a few hours. More importantly, the advanced focused ion beam (FIB) and the low-dose high-resolution transmission electron microscopy (HRTEM) imaging technique have been utilized for unraveling the zeolite heterojunction at the atomic level during the epitaxial growth process. It turns out (222) crystallographic planes of the **SOD**-type zeolite substrate provide unique pre-building units, which facilitate the growth of targeted ABC-6 family small pore zeolites along its c-axis. Moreover, the morphologies of **ERI-**type zeolite can also be tuned through the epitaxial growth approach, achieving a longer lifetime in the methanol conversion.

Conventional zeolites are a type of crystalline porous materials composed of TO_4 tetrahedra (T = Si and Al) linked by bridging oxygen, forming well-defined channels and/or cavities of different sizes and shapes. Based on pore openings delimited by T atoms, they can be further categorized into small pore (8 T), medium pore (10 T), large pore (12 T), and even extra-large pore (≥12 T) zeolites [1–6]. Typically, small, medium, and large pore zeolites have corresponding pore diameters of approximately 3.8 Å, 5.3 Å, and 7.4 Å, respectively. Until now, there have been 257 framework type codes (FTCs) approved by the international zeolite association – structural committee. Nowadays, research interests have been focused on the small pore zeolites due to their promising applications in upgrading small molecules, methanol to olefins, catalytic environmental remediation, *etc.* [7–15]. For instance, inorganic cations exchanged small pore 8 × 8 × 8-ring SSZ-13 (**CHA**) zeolites with order *cha* cages have displayed the highest selectivity of CO_2 over CH_4, which can be explained by the "molecular trapdoor" mechanism [16]. Furthermore, Cu-exchanged small pore SSZ-13 (**CHA**), SSZ-16 (**AFX**), SSZ-39 (**AEI**) zeolites have shown the promising selective catalytic reduction (SCR) of NO_x [17–21]. Therefore, it stimulates researchers from industry and academia to synthesize small pore zeolites with targeted topologies in a short crystallization time.

Typically, small-pore zeolites can be synthesized by employing traditional silica sources (such as silica sol, ethyl orthosilicate, water glass) and alumina sources (such as sodium aluminate, aluminum hydroxide, aluminum isopropoxide) in the presence of inorganic or/and organic structure-directing agents (SDAs) under hydrothermal conditions (Scheme 1a) [22–26]. Recently, **FAU**-type zeolite with different Si/Al ratios are frequently utilized as raw ma-

* Corresponding authors.
E-mail addresses: daliang.zhang@cqu.edu.cn (D. Zhang), pguo@dicp.ac.cn (P. Guo).
[1] These authors contributed equally to this work.

https://doi.org/10.1016/j.cclet.2023.108470
1001-8417/

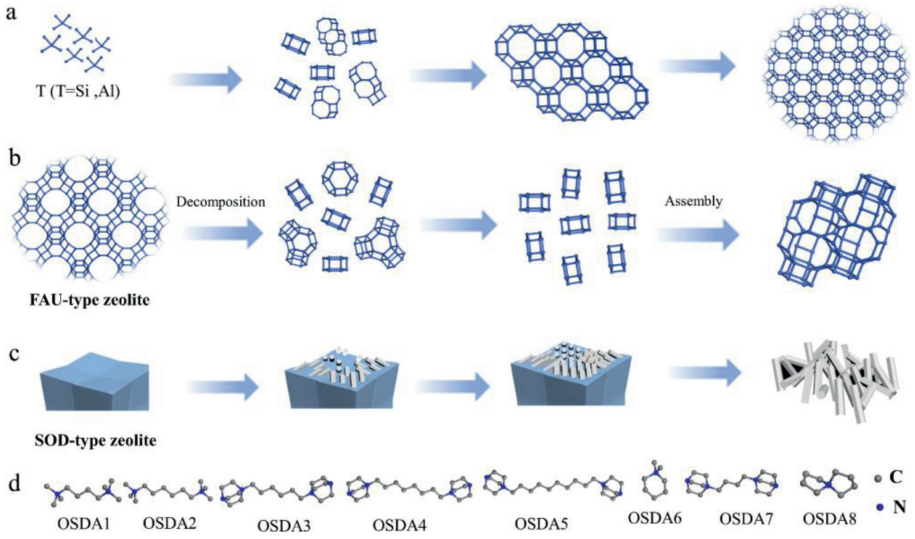

Scheme 1. (a) Utilization of conventional silicon and aluminum sources for synthesizing small pore zeolites [22]. (b) Synthesis of small pore zeolites using **FAU-**type zeolites as silicon and aluminum sources [27]. (c) Design ABC-6 family small pore zeolites through the epitaxial growth on another ABC-family zeolite. (d) OSDAs utilized in this work.

terials for fabricating such small pore zeolites with tailored properties (Scheme 1b) [27–31]. For example, Cu-exchanged **AEI**-type small pore zeolite SSZ-39, which displays the promising SCR catalytic performance, can be efficiently synthesized by employing **FAU**-type zeolite as raw materials [31]. Moreover, it is worth noting that most of such significant small pore zeolites belong to the hexagonal ABC-6 family, which are constructed by stacking layers of three kinds of 6-rings (denoted as A, B and C) parallel to the *ab*-plane linked by 4-rings along the *c*-axis [3]. Therefore, the judicious selection of one ABC-6 family member as the parent material, might be an alternative approach for the targeted synthesis of other ABC-6 family members (Scheme 1c). For example, Tatsuya Okubo et al. demonstrated that introducing **SOD**-type zeolite (Si/Al = 1) into the initial gel can facilitate the epitaxial growth of **CAN**- and **CHA**-type zeolites on its surface. However, the further growth of **CAN** and **CHA**-type zeolites is frequently impeded, resulting in the formation of **CHA-SOD** and **CHA-SOD** heterostructures instead. While the relative orientations between the substrate (**SOD**-type zeolite) and newly grown zeolites (**CAN**- and **CHA**-type zeolites) were identified, there has been no direct observation of zeolite heterojunctions at the atomic level [32,33].

In this study, we present a novel synthetic method called the epitaxial growth approach for designing small pore zeolites of the ABC-6 family. Unlike conventional epitaxial growth methods that necessitate supplementary starting materials, we utilized the substrate itself as the source material for the growth process, which took place after substrate dissolution. To achieve this approach, inorganic cations such as Na^+ and K^+ are combined with various organic structure directing agents (OSDAs) during epitaxial growth on nonporous **SOD**-type zeolite, which serves as the sole source of silica and aluminum. Using this approach, we have successfully synthesized **ERI**-, **SWY**-, **LEV**-, **AFX**- and **PTT**-type zeolites belonging to the ABC-6 family in just a few hours. The advanced focused ion beam (FIB) and low-dose high-resolution transmission electron microscopy (HRTEM) imaging techniques were utilized to study the zeolite heterojunction during the epitaxial growth process at the atomic level.

The nonporous aluminosilicate **SOD**-type zeolite with ABC stacking sequence (Si/Al = 10) is selected as the substrate, which can be easily obtained by the grinding method (Fig. S1 in Supporting information). The as-synthesized **SOD**-type zeolite with the well-defined cubic morphology in micrometer will further facilitate the growth of new zeolites (Figs. 1a and b). The small pore **ERI**-type zeolite with AABAAC stacking sequence was firstly selected, in which there are double 6-rings (*d6r*), *can*, and *eri* cages as composite building units (CBUs) as demonstrated in Fig. 2a. It was synthesized using aluminosilicate **SOD**-type zeolite as the sole silica and aluminum sources in the presence of K^+ and diquaternary ammonium OSDA1 (Scheme 1d) [34]. The pure-phase and well-crystallized **ERI**-type zeolite (denoted as ERI-4C) were rapidly synthesized in only 4 h (Fig. S2 in Supporting information). Similarly, we also utilized OSDA2 [26,35] and the K^+ as inorganic SDA and OSDA to synthesize **ERI**-type zeolite (designated ERI-6C). Well-crystallized and pure-phase ERI-6C could be completely generated

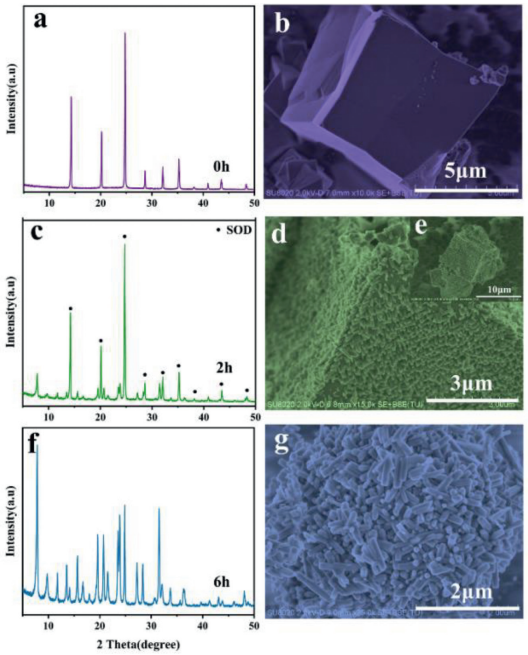

Fig. 1. (a, b) PXRD and SEM image of fresh **SOD-**type zeolite. (c-e) PXRD and SEM images of ERI-6C crystallized for 2 h (the unreacted **SOD-**type zeolite is marked in the PXRD pattern, and the insert is the corresponding low magnification). (f, g) PXRD and SEM image of ERI-6C crystallized for 6 h.

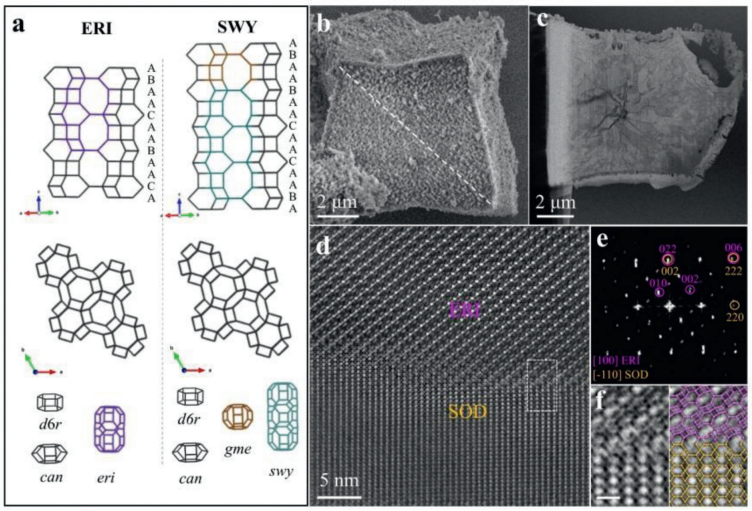

Fig. 2. (a) Stacking orders and CBUs in **ERI** and **SWY** framework. (b) SEM image of an ERI-6C crystal, in which a marked line indicates the location of TEM lamella. (c) The TEM image taken from the lamella prepared by using FIB. (d) The CTF corrected HRTEM image obtained from the interface between **ERI-** and **SOD-**type zeolites. (e) The corresponding FFT pattern of (d) with reflections indexed by **ERI** (pink) and **SOD** (yellow) structures. (f) A cropped and enlarged image from (d) as indicated by the white rectangle and the same image overlaid with a proposed structural model at the interface (**ERI** in pink, **SOD** in yellow). Scale bar: 1 nm.

within 6 h (Figs. 1f and g). It is of interest to note that the diameter of rod in the ERI-4C (Fig. S2i) is 50 nm approximately, which is smaller than the one of ERI-6C (Fig. 1g). Table S1 (Supporting information) demonstrates that ERI-4C and ERI-6C possess comparable Si/Al ratios (5.45 *vs.* 4.93). The BET surface areas for ERI-4C and ERI-6C are 515.21 and 444.47 m^2/g, respectively (Table S2 in Supporting information), and Fig. S3 (Supporting information) displays their pore size distributions.

The crystallization process of ERI-6C is monitored by powder X-ray diffraction (PXRD) and scanning electron microscopy (SEM). After a hydrothermal synthesis period of 2 h, both **SOD**- and **ERI**-type zeolites are present, as reflected in the PXRD shown in Fig. 1c. SEM images (Figs. 1d and e) illustrate that the **ERI**-type zeolite grows on the surface of **SOD**-type one. Interestingly, the substrate **SOD**-type zeolite completely disappears and transforms into well-crystallized **ERI**-type ones with hexagonal nanorod morphologies within 6 h (Figs. 1f and g). In order to probe the heterojunction structure at the interface of **ERI**- and **SOD**-type zeolite at the atomic level, the modern focused ion beam (FIB) instrument offering the capability to tilt and rotate selected crystals of interest was employed. Therefore, we could prepare the TEM lamellas according to the [110] zone axis of the **SOD**-type zeolite substrate (Figs. 2b and c). Subsequently, the low-dose high-resolution transmission electron microscopy (HRTEM) imaging technique [36] is performed at the interface region (Fig. 2d). As indexed in its corresponding FFT pattern shown in Fig. 2e, it indicates that the HRTEM image was taken along the [100] zone axis of **ERI**-type zeolite and the [-110] zone axis of **SOD**-type are zeolite substrate. Moreover, the FFT pattern also shows the 00*l* reflections of **ERI** are aligned with the *hhh* reflections of **SOD**. It indicates that both the [111] direction of **SOD** and the [001] one of **ERI** are ABC 6-ring stacking orientations and also illustrates that the specific (222) crystallographic planes of **SOD**-type zeolite substrates provide the unique locations for the further growth of the targeted **ERI**-type zeolite along its *c*-axis. In addition, it is worth noting that the 0*kk* reflections of the **ERI** were perfectly aligned with the 00*l* reflections of the **SOD** in this **ERI**-**SOD** zeolite heterojunction (Fig. 2e). This suggests that the **ERI**-type zeolite may also grow through its (022) crystallographic plane onto the (002) surface of the **SOD**-type zeolite substrate. The CTF-corrected HRTEM image at the thinnest part of the interface shows the atomic locations of T atom columns, enabling the construction of an interface model for both framework structures (Fig. 2f and Fig. S4 in Supporting information). The model reveals that the **SOD**-type zeolite substrate, terminated by 6-rings, is connected to the **ERI** framework by 4-rings (Fig. 2f and Fig. S5 in Supporting information). Additionally, every third 6-ring in the **SOD**-type zeolite breaks and merges with an 8-ring of the **ERI** framework, resulting in larger pore openings and dangling silanol groups.

We have successfully synthesized **ERI**-type zeolite within a short crystallization time using the epitaxial growth approach on **SOD**-type zeolite. This achievement has sparked curiosity about the potential application of this methodology to other members of the ABC-6 family. We selected **SWY**-type zeolite as the next target, as both **ERI** and **SWY** frameworks belong to the hexagonal crystal system, have the same *a* and *b* unit cell parameters, and possess the common *d*6*r* and *can* CBUs. The stacking sequence of the **SWY** framework is AABAABAACAAC (Fig. 2a). **SWY**-type aluminosilicate zeolites were firstly reported in 2021 and could be synthesized by using OSDA3-OSDA5 in the presence of inorganic K^+ and tetrapropylammonium hydroxide (TPAOH) as co-templates [37]. In our work, we used OSDA3-OSDA5 and KOH to design **SWY**-type aluminosilicates through epitaxial growth on **SOD**-type zeolite. The experimental results show that **SWY**-type zeolites (denoted as SWY-6C, SWY-8C and SWY-10C) can be completely generated within only 6–10 h without the use of TPAOH (Fig. S6 in Supporting information), greatly accelerating the crystallization time compared to previous reports. Moreover, the corresponding Si/Al, BET surface area, and pore size distribution of **SWY**-type zeolites are given in Tables S1 and S2, Fig. S7 (Supporting information).

Both **ERI**- and **SWY**-type zeolites crystallize in the presence of K^+ ions as inorganic cations. We also investigate the synthesis of other ABC-6 family small pore zeolites through epitaxial growth on the **SOD**-type zeolite in the presence of Na^+ cations. The small pore aluminosilicate **LEV**-type zeolite containing *d*6*r* and *lev* cages as CUBs (AABCCABBC stacking sequence) was selected as shown in Fig. 3a. Using Na^+ ions and OSDA6 as SDAs [38], the pure-phase **LEV**-type zeolites can be successfully synthesized within 6 h (denoted as LEV, Si/Al = 7.84). BET surface area and pore sizes distribution of LEV samples are shown in Table S2 and Fig. S8 (Supporting information), respectively. We systematically investigated the crystallization process (Fig. S9 in Supporting information). Our results indicate that the **LEV**-type zeolite initially grow on the surface of the **SOD**-type zeolite, after which the **SOD**-type zeolite substrate dissolves and completely converts into our target **LEV**-type zeo-

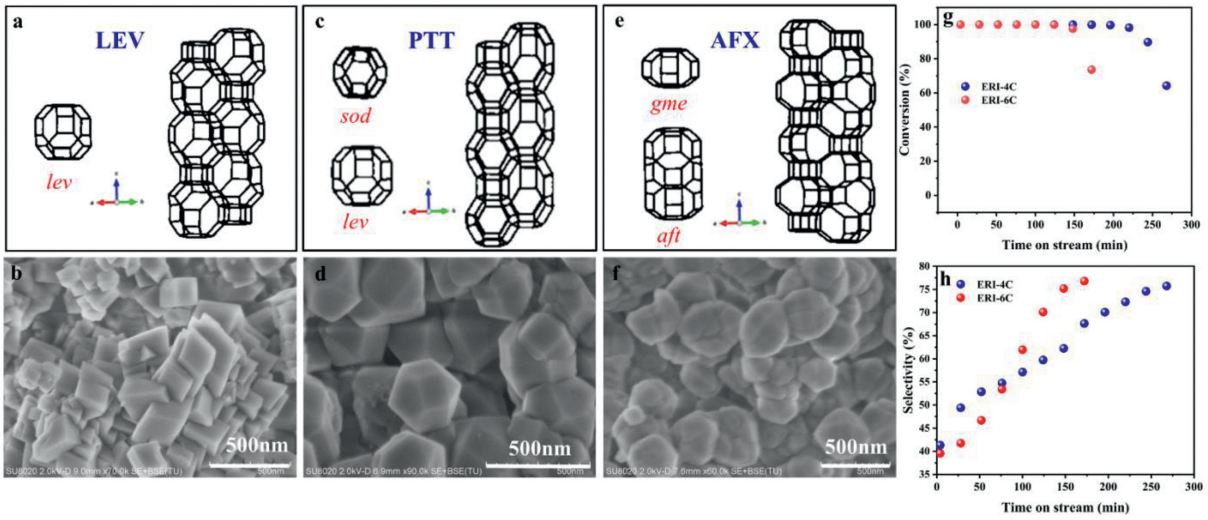

Fig. 3. (a, b) **LEV** framework and **LEV**-type zeolite morphology. (c, d) **PTT** framework and **PTT**-type zeolite morphology. (e, f) **AFX** framework and **AFX**-type zeolite (AFX-4C) morphology. (g, h) MTO catalytic performance of ERI-4C and ERI-6C.

lite with a particle size of approximately 300 nm (Fig. 3b). The advanced FIB and low-dose HRTEM imaging techniques were also performed on the investigation of the interface structure at the atomic level. It turns out that (009) reflection of **LEV** is exactly overlapped with 222 reflection of **SOD**, which indicates that the targeted **LEV**-type zeolite grows along its *c*-axis based on (222) crystallographic planes of **SOD**-type zeolite substrates (Fig. S10 in Supporting information). This scenario is quite similar to the one observed in the case of **ERI**-**SOD**.

In addition, aluminosilicate small pore **AFX**- and **PTT**-type zeolites can also be fabricated using **SOD**-type zeolite as substrates in the presence of Na^+ cations and OSDA7-8 [39,40], respectively. SEM images and PXRD patterns (Figs. S11 and S12 in Supporting information) confirm that both zeolites are synthesized on the surface of **SOD**-type zeolite, followed by complete conversion of the **SOD**-type zeolite substrate into the target zeolite within a few hours. For the **PTT**-type zeolite, it was firstly reported in 2020 by utilizing OSDA8 with the hexagonal flake morphologies in microsize. From the structural point of view, it contains the alternating *lev* CBUs column and *d*6*r*-*sod* column along the *c*-axis, generating a unique 2D channel system with the AABC stacking sequence (Fig. 3c). Using our synthetic methodology reported in this work, **PTT**-type zeolite (denoted as PTT) with polyhedron morphologies (about 300 nm or even smaller) could be synthesized within 8 h (Fig. 3d). Moreover, the universality of this approach can also be reflected in **AFX**-type zeolite using OSDA7. It is composed of *d*6*r*, *gme*, and *aft* cages as CUBs, generating the AABBCCBB stacking sequence as displayed in Fig. 3e. Using the epitaxial growth approach, **AFX**-type zeolites (denoted as AFX-4C) with the polyhedral morphologies were successfully obtained (Fig. 3f). Table S1 displays the Si/Al ratios for the AFX-4C (3.89) and PTT (4.48) samples, while Table S2 shows that the BET surface areas for AFX-4C and PTT samples are 508.40 and 278.53 m^2/g, respectively. The pore size distributions of AFX-4C and PTT samples are depicted in Figs. S13 and S14 (Supporting information), respectively.

We also test the MTO catalytic performance of **ERI**-type and **AFX**-type zeolites. As shown in Fig. 3g, compared with ERI-6C, ERI-4C catalyst exhibits a longer lifetime. Selected area electron diffraction (SAED) was conducted on the ERI-4C and ERI-6C catalysts, and the results revealed that the *ab*-plane (8-ring pore openings) runs across the diameter of the rod (Fig. S15 in Supporting information). It was observed that as the diameter of the rod decreases, the diffusion path becomes shorter. The rods in ERI-4C and ERI-6C have diameters of approximately 50 nm and 100 nm, respectively (Fig. 1g and Fig. S2i), indicating that ERI-4C has a shorter diffusion path than ERI-6C. The ERI-4C catalyst's longer lifetime was attributed to its shorter diffusion path, as the main products could diffuse out of the catalysts more easily, which suppressed its deactivation. The selectivity of light olefins including ethene and propylene over the ERI-4C catalyst is up to 74.6% (Fig. 3h). Moreover, compared with **AFX**-type zeolite prepared by employing **FAU**-type zeolites as silicon and aluminum sources (denoted as AFX-from-FAU), the one synthesized by our epitaxial growth approach displays a slightly increasing selectivity of light olefins in the MTO reaction (Fig. S16 in Supporting information).

In summary, we propose an efficient method for designing small pore zeolites belonging to the ABC-6 family, using the epitaxial growth approach on nonporous **SOD**-type zeolite as substrates. The atomic structure at the interface of zeolite heterojunctions was systematically investigated using FIB and low-dose HRTEM imaging techniques in this work. This synthetic methodology has great potential for expanding the synthesis of other ABC-6 zeolite family members and even designing novel structures within this family.

Declaration of competing interest

The authors declare that they have no known competing financial interests or personal relationships that could have appeared to influence the work reported in this paper.

Acknowledgments

This work is supported by National Key Research and Development Project of China (No. 2022YFE0113800), National Natural Science Foundation of China (Nos. 22288101, 21972136, 21991090 and 21991091), and Key Research Program of Frontier Sciences, Chinese Academy of Sciences (No. QYZDB-SSW-JSC040).

Supplementary materials

Supplementary material associated with this article can be found, in the online version, at doi:10.1016/j.cclet.2023.108470.

References

[1] Y. Li, J. Yu, Chem. Rev. 114 (2014) 7268–7316.
[2] C. Ma, X. Liu, C. Nie, et al., Chem. J. Chin. Univ. 42 (2021) 188–200.

[3] P. Guo, N. Yan, L. Wang, X. Zou, Cryst. Growth Des. 17 (2017) 6821–6835.
[4] M. Moliner, C. Martinez, A. Corma, Angew. Chem. Int. Ed. 54 (2015) 3560–3579.
[5] M. Moliner, F. Rey, A. Corma, Angew. Chem. Int. Ed. 52 (2013) 13880–13889.
[6] T. Pang, X. Yang, C. Yuan, et al., Chin. Chem. Lett. 32 (2021) 328–338.
[7] R. Bai, X. Song, W. Yan, J. Yu, Natl. Sci. Rev. 9 (2022) nwac064.
[8] F. Chen, Y. Li, A. Huang, Chin. Chem. Lett. 32 (2021) 1086–1088.
[9] Y. Li, J. Yu, Nat. Rev. Mater. 6 (2021) 1156–1174.
[10] P. Tian, Y. Wei, M. Ye, Z. Liu, ACS Catal. 5 (2015) 1922–1938.
[11] P. Ferri, C. Li, R. Millan, et al., Angew. Chem. Int. Ed. 59 (2020) 19708–19715.
[12] Y. Shan, J. Du, Y. Zhang, et al., Natl. Sci. Rev. 8 (2021) nwab010.
[13] A.M. Beale, F. Gao, I. Lezcano-Gonzalez, C.H. Peden, J. Szanyi, Chem. Soc. Rev. 44 (2015) 7371–7405.
[14] N. Yan, C. Ma, Y. Cao, et al., Small 16 (2020) 2000902.
[15] C. Bian, D. Li, Q. Liu, et al., Chin. Chem. Lett. 33 (2022) 1169–1179.
[16] J. Shang, G. Li, R. Singh, et al., J. Am. Chem. Soc. 134 (2012) 19246–19253.
[17] C. Paolucci, I. Khurana, A.A. Parekh, et al., Science 357 (2017) 898–903.
[18] M. Chen, J. Li, W. Xue, et al., J. Am. Chem. Soc. 144 (2022) 12816–12824.
[19] R. Li, X. Jiang, J. Lin, et al., Chem. Eng. J. 441 (2022) 136021.
[20] M. Moliner, C. Franch, E. Palomares, M. Grill, A. Corma, Chem. Commun. 48 (2012) 8264–8266.
[21] J. Du, Y. Shan, Y. Sun, et al., Appl. Catal. B: Environ. 294 (2021) 120237.
[22] S.H. Ahn, H. Lee, S.B. Hong, Chem. Mater. 29 (2017) 5583–5590.
[23] Y. Tong, D. Yuan, W. Zhang, et al., J. Energy Chem. 58 (2021) 41–47.
[24] H. Lee, J. Zeng, A. Mayoral, S.B. Hong, J. Am. Chem. Soc. 144 (2022) 18700–18709.
[25] H. Lee, J. Shin, K. Lee, et al., Science 373 (2021) 104–107.
[26] J.H. Lee, M.B. Park, J.K. Lee, et al., J. Am. Chem. Soc. 132 (2010) 12971–12982.
[27] D.V. Bruter, V.S. Pavlov, I.I. Ivanova, Pet. Chem. 61 (2021) 251–275.
[28] K. Muraoka, Y. Sada, A. Shimojima, W. Chaikittisilp, T. Okubo, Chem. Sci. 10 (2019) 8533–8540.
[29] X. Zhang, Y. Wang, X. Wang, et al., Microporous Mesoporous Mater. 279 (2019) 407–415.
[30] R. Li, Y. Zhu, Z. Zhang, et al., Appl. Catal. B: Environ. 283 (2021) 119641.
[31] H. Xu, L. Zhu, Q. Wu, X. Meng, FS. Xiao, Inorg. Chem. Front. 9 (2022) 1047–1057.
[32] T. Okubo, T. Wakihara, J. Plévert, et al., Angew. Chem. Int. Ed. 40 (2001) 1069–1071.
[33] T. Wakihara, S. Yamakita, K. Iezumi, T. Okubo, J. Am. Chem. Soc. 125 (2003) 12388–12389.
[34] C.R. Boruntea, G. Sastre, L.F. Lundegaard, A. Corma, P.N.R. Vennestrøm, Chem. Mater. 31 (2019) 9268–9276.
[35] J. Zhu, Z. Liu, K. Iyoki, et al., Chem. Commun. 53 (2017) 6796–6799.
[36] D. Zhang, Y. Zhu, L. Liu, et al., Science 359 (2018) 675–679.
[37] R.G. Chitac, J. Bradley, N.D. McNamara, et al., Chem. Mater. 33 (2021) 5242–5256.
[38] N. Funase, T. Tanigawa, Y. Yamasaki, et al., J. Mater. Chem. A 5 (2017) 19245–19254.
[39] H. Yamada, T. Iida, Z. Liu, et al., Cryst. Growth Des. 16 (2016) 3389–3394.
[40] H. Lee, W. Choi, H.J. Choi, S.B. Hong, ACS Mater. Lett. 2 (2020) 981–985.